Atmos. Chem. Phys., 11, 3879–3894, 2011
www.atmos-chem-phys.net/11/3879/2011/
doi:10.5194/acp-11-3879-2011

Atmospheric Chemistry and Physics

SOA from limonene: role of NO_3 in its generation and degradation

J. L. Fry[1,*], A. Kiendler-Scharr[2], A. W. Rollins[1], T. Brauers[2], S. S. Brown[3], H.-P. Dorn[2], W. P. Dubé[3], H. Fuchs[3,], A. Mensah[2,***], F. Rohrer[2], R. Tillmann[2], A. Wahner[2], P. J. Wooldridge[1], and R. C. Cohen[1]**

[1]Department of Chemistry, University of California, Berkeley, CA, USA
[2]IEK 8: Troposphäre, Forschungszentrum Jülich, 52425 Jülich, Germany
[3]Chemical Sciences Division, NOAA Earth System Research Laboratory, Boulder, CO, USA
[*]current address: Chemistry Department, Reed College, Portland, OR, USA
[**]current address: IEK 8: Troposphäre, Forschungszentrum Jülich, 52425 Jülich, Germany
[***]current address: Institute for Atmospheric and Climate Science, ETH Zürich, Zürich, Switzerland

Received: 6 December 2010 – Published in Atmos. Chem. Phys. Discuss.: 22 December 2010
Revised: 9 April2011 – Accepted: 12 April 2011 – Published: 28 April 2011

Abstract. The formation of organic nitrates and secondary organic aerosol (SOA) were monitored during the NO_3 + limonene reaction in the atmosphere simulation chamber SAPHIR at Research Center Jülich. The 24-h run began in a purged, dry, particle-free chamber and comprised two injections of limonene and oxidants, such that the first experiment measured SOA yield in the absence of seed aerosol, and the second experiment yields in the presence of 10 $\mu g\, m^{-3}$ seed organic aerosol. After each injection, two separate increases in aerosol mass were observed, corresponding to sequential oxidation of the two limonene double bonds. Analysis of the measured NO_3, limonene, product nitrate concentrations, and aerosol properties provides mechanistic insight and constrains rate constants, branching ratios and vapor pressures of the products. The organic nitrate yield from NO_3 + limonene is ≈30%. The SOA mass yield was observed to be 25–40%. The first injection is reproduced by a kinetic model. PMF analysis of the aerosol composition suggests that much of the aerosol mass results from combined oxidation by both O_3 and NO_3, e.g., oxidation of NO_3 + limonene products by O_3. Further, later aerosol nitrate mass seems to derive from heterogeneous uptake of NO_3 onto unreacted aerosol alkene.

1 Introduction

Biogenic volatile organic compounds (BVOCs) make up a large fraction of gas-phase organic compounds emitted to the atmosphere: on a global scale, vegetation emissions of VOCs are an order of magnitude greater than those from petrochemicals (Guenther et al., 1995). Furthermore, in the atmosphere, many of these compounds are rapidly oxidized and likely to form condensable products (Griffin et al., 1999). Among these compounds, monoterpenes are known to be important sources of secondary organic aerosol (SOA) (Goldstein and Galbally, 2007; Eerdekens et al., 2009; Tunved et al., 2006; Slowik et al., 2010; Hallquist et al., 1999).

If NO_3-initiated aerosol formation from biogenic VOCs is a significant contribution to organic aerosol loading in the atmosphere, this would provide a potential resolution to a paradox noted in the SOA literature: ^{14}C measurements show the carbon in organic aerosol to be primarily modern, which is characteristic of natural emissions, from urban (≈50%) to remote areas (80–100%) (Schichtel et al., 2008). However, aerosol loading in both urban and rural areas is observed to be correlated to aging in anthropogenic emissions plumes (de Gouw et al., 2005; Quinn et al., 2006; Weber et al., 2007). NO_3 produced BVOC SOA resolves the paradox by requiring both an anthropogenic oxidant "trigger" and biogenic VOC to form aerosol (Hoyle et al., 2011). This mechanism of SOA formation is expected to be most significant in forested areas downwind of urban centers or power plants, where NO_x is high and biogenic VOCs are abundant (Pye et al., 2010). Because the nitrate radical is photolabile, this mechanism is also expected to be most important at night or within a shaded forest canopy.

Limonene is of interest as a representative BVOC both due to its high emission rate among monoterpenes (Sakulyanontvittaya et al., 2008) and its possession of two double bonds. These two reactive sites for oxidation give limonene a rapid and direct route to the types of low-vapor pressure oxidized products that are likely to form secondary organic aerosol. As a consequence, limonene may contribute disproportionately to total SOA relative to other

Correspondence to: R. C. Cohen
(rccohen@berkeley.edu)

terpenoids (Lane et al., 2008; Maksymiuk et al., 2009). Further, limonene's frequent use in household cleaning products and air fresheners makes it a common source of indoor air pollution when its oxidation results in aerosol formation (Wainman et al., 2000). Aerosol formation from the reaction of NO_3 with limonene has been the subject of a previous chamber study (Spittler et al., 2006); in excess limonene and no O_3, organic nitrates were formed in high yield (67%), accompanied by immediate SOA formation.

Here we report chamber measurements and kinetic modeling of gas- and aerosol-phase chemistry during SOA formation initiated by the NO_3 + limonene reaction under excess oxidants.

2 Experimental

2.1 Atmosphere simulation chamber SAPHIR

The experiment described below was conducted on 16 and 17 June 2007 in the atmospheric simulation chamber SAPHIR at Research Center Jülich as part of the intercomparison campaign of NO_3 (Dorn et al., 2011), N_2O_5 (Apodaca et al., 2011), and NO_2 (Fuchs et al., 2009) measurements. The SAPHIR chamber is a large (270 m^3) cylindrical chamber with double walls made from FEP film. It is equipped with an automated shuttering system to enable simulation of day or night conditions. The chamber and its operation during simulation experiments has been described in detail (e.g. Rohrer et al., 2005; Bohn and Zilken, 2005; Wegener et al., 2007). The chamber was used for large instrument intercomparison campaigns (e.g. Apel et al., 2008; Schlosser et al., 2009) and it was shown to serve as an excellent platform for multi-instrument experiments. Only a brief description of the chamber instruments and chamber operation is presented in the following.

The chamber has standard instrumentation for measurement of NO (chemiluminescence), NO_x, temperature, pressure, humidity, dilution flow, and O_3 (UV-absorption). However, during this experiment ozone concentrations were measured by chemiluminescence in a modified ECO Physics CLD AL 700 (Ridley et al., 1992). A GC-FID system (Perkin-Elmer) was used to verify the cleanness after purging and to follow the ethane concentration as an inert tracer of dilution. The limonene concentration was measured by Proton Transfer Reaction Mass Spectrometry (PTR-MS, IONICON, Austria; Lindinger et al., 1998).

Before the experiment, the chamber was purged overnight to parts per trillion (ppt) levels of nitrogen oxides, ozone, and hydrocarbons using a large flow 300 m^3/h of clean synthetic air (N_2, O_2, purity > 99.9999%). During the experiment, the pressure was maintained at 30–50 hPa above ambient to prevent contamination. The slight overpressure was held by a smaller replenishment flow of the same synthetic air as used for flushing. During the entire experiment a fan provided fast mixing of constituents within the chamber. Due to the replenishment flow of 10–15 m^3/h all gases were diluted by a rate of ≈4–5.5 %/h. The shutter system was closed throughout the experiment, keeping the chamber in darkness.

The trace gases (NO_2, ethane, and limonene) were added to the replenishment flow. Ozone (≈5 %) was produced by silent discharge in pure oxygen and injected into the chamber. Before the reaction started, 500 ppm of CO was added to the chamber in order to scavenge any OH formed.

2.2 NO_3, N_2O_5, and NO_{yi} measurements

During the intercomparison campaign several instruments measuring NO_3 and N_2O_5 concentrations were operated at SAPHIR (Dorn et al., 2011; Apodaca et al., 2011). Here we employ the data set from one of the instruments, the Cavity Ring-Down Spectrometer (CRDS) of the NOAA Earth System Research Lab team (Dube et al., 2006; Fuchs et al., 2008). None of the conclusions of this manuscript depend strongly on the choice of the $NO_3 + N_2O_5$ measurement, as all measurements agreed to within 20%.

NO_2 was measured by laser-induced fluorescence (LIF) and total peroxynitrates (ΣPNs), total alkyl and multifunctional nitrates (ΣANs), and nitric acid (HNO_3) were determined using thermal dissociation to NO_2 in heated quartz ovens held at different temperatures ("NO_2-TD-LIF") (Thornton et al., 2000; Day et al., 2002). Details of this instrument are described in Wooldridge et al. (2010).

Briefly, the NO_2-TD-LIF instrument sampled at 3 standard liters per minute (slpm) from ca. 10 cm above the floor of the SAPHIR chamber through a Teflon PFA inlet (40 cm of 3.2 mm inner diameter tubing). A glass capillary orifice was used to reduce pressure, and the sample was split to four channels. In the ambient temperature channel NO_2 is detected. The other channels are held at 180 °C, 350 °C, and 600 °C,where ΣPNs, ΣANs, and HNO_3 dissociate to yield NO_2. The mixing ratio of each class of nitrate is calculated from the difference in total NO_2 measured in adjacent temperature channels. We expect both gaseous and semivolatile aerosol-phase nitrates to dissociate completely, while thermally stable salts such as $NaNO_3$ will not be detected.

The NO_2 concentration in the reduced-pressure sample flow (P≈1.5 Torr, 200 Pa) is detected by LIF. Here, we excite with a 408 nm continuous-wave diode laser at (8 mW, Toptica Photonics DL100) and collect filtered red-shifted fluorescence (λ>650 nm) with a photomultiplier tube (PMT, Hamamatsu H7421-50) mounted at 90° to both the laser and sample flow. This instrument employed two detection cells, with detection limits of ≈90 ppt 10 s^{-1} for NO_2 and ≈250 ppt 10 s^{-1} for ΣPNs, ΣANs, and HNO_3. The lower sensitivity for higher oxides accounts for noise associated with subtraction of the up to 40 parts per billion (ppb) NO_2 present in these experiments. Detection limits for this instrument were calculated as described by Day et al. (2002).

2.3 AMS and other particle instrumentation

An aerosol mass spectrometer (Aerodyne TOF-AMS) was operated to measure the aerosol chemical composition. The AMS was connected to the SAPHIR chamber via a stainless steel tube to minimize losses in the sampling line. The AMS working principles and modes of operation are explained in detail elsewhere (Canagartna et al., 2007). In brief, an aerodynamic lens system at the instrument inlet is used to remove gas and supermicron particles from the sample flow, while submicron particles are impacted on a tungsten vaporizer which is held at ≈600 °C. The resulting vapors are ionized with 70 eV electron impact ionization. A time of flight mass spectrometer is used for high resolution analysis of the chemical composition of these ions.

For the extraction of chemically resolved mass concentrations of individual species the AMS raw data are typically evaluated with standard assumptions as described by Allan et al. (2004). This approach makes use of the reproducibility of mass spectral patterns of typical inorganic aerosol components such as ammonium, sulphate and nitrate. Subtracting from a measured mass spectrum the contributions of inorganic constituents and the contribution of gas phase sample, which is exclusively composed of N_2, O_2, H_2O and gases with mixing ratios in the ppm range, one obtains the mass spectrum of the organic aerosol. Due to the non-selective ionization with electron impact at 70 eV used in the AMS and the high fragmentation induced, further identification of individual molecules in a complex organic component is not possible. However, positive matrix factorization can be employed to obtain information about different chemical species (see below). Furthermore the assumptions on inorganic aerosol fragmentation patterns can be tested explicitly and revised where necessary. Inorganic nitrate from e.g. NH_4NO_3 is detected as NO^+ (*m/z* 30) and NO_2^+ (*m/z* 46) with a typical ratio of NO_2^+:NO^+ of 0.35. In the W-mode (high mass resolution) of the TOF-AMS, possible interferences on mass to charge ratios 30 (e.g. CH_2O^+) and 46 (e.g. $CH_2O_2^+$) can be identified and accounted for in the further data evaluation. This option has been used for the experiments described here to derive the nitrate content and identity of the SOA. The quantification of the nitrate content of the SOA was performed based on calibrations with NH_4NO_3 aerosol. The observed ratio of NO_2^+:NO^+ for SOA was 0.15 +/− 0.02 which is considerably lower than 0.35 throughout the experiments indicating that the aerosol did not contain significant amounts of inorganic nitrate or nitric acid. Nitrate quantification was performed under the following assumptions: the collection efficiency of the aerosol was set to one, in agreement with previous studies on NO_3 + β-pinene (Fry et al., 2009) and NO_3 + isoprene (Rollins et al., 2009) SOA formation. The relative ionization efficiency (RIE) of the organics was set to 1.4 which is the standard value in AMS analysis, and the RIE of nitrate was set to 1, assuming organic nitrates are ionized equally efficiently to NH_4NO_3.

Aerosol number concentrations were measured with a Water Condensation Particle Counter (TSI WCPC model 3785). To determine aerosol wall loss rate, we use the loss rate determined by an exponential fit of the decay of CPC-measured aerosol number concentration after it has peaked 10 h into the experiment, after the second limonene injection. The peak concentration was 70 000 particles cm^{-3}, after which decay was steady. This fit gives an effective aerosol loss rate of $\approx 7 \times 10^{-5}\ s^{-1}$, or an effective aerosol chamber lifetime of ≈4 h.

3 Results

Figure 1 displays an overview of the NO_3 + limonene experiment. It was only possible to conduct this comprehensive experiment once during NO_3Comp, the 2007 NO_3 instrument intercomparison campaign. We hope our analysis will inspire additional studies of this and related systems.

All time axes are shown in hour since the beginning of the experiment, which commenced (hour 0) at 06:00 UTC on 16 July 2007. The experiment was initiated after the SAPHIR chamber had been purged overnight with clean, dry air. At 26 min into the experiment (label (a) in Fig. 1), 10 ppb of limonene was introduced to the chamber by adding the appropriate volume of liquid, along with 22 ppb of NO_2. Reactive chemistry was initiated approximately 2.5 h later (label (b) in Fig. 1) by the addition of NO_2 to bring the concentration up to 28 ppb along with 38 ppb of O_3. After this point, NO_3 and N_2O_5 are produced in the chamber by the following reactions:

$$NO_2 + O_3 \rightarrow NO_3 + O_2 \quad \text{(R1)}$$

$$NO_3 + NO_2 \rightarrow N_2O_5 \quad \text{(R2)}$$

$$N_2O_5 \rightarrow NO_3 + NO_2 \quad \text{(R3)}$$

The sum $N_2O_5 + NO_3$ is the total NO_3 reservoir, because as NO_3 is depleted, N_2O_5 decomposes rapidly to replenish NO_3 (Reaction R3).

Both O_3 and NO_3 react with the limonene, resulting in complete consumption of limonene within 2.5 h. Gas- and aerosol-phase organic nitrates are formed immediately upon initiation of this reactive stage of the experiment, with aerosol-phase nitrates increasing markedly after oxidation of the second double bond (at approximately 5 h and 10 h for the two injections). The apparent negative alkyl nitrate observations after the first injection (around hour 3 of the experiment, Fig. 1 lower panel) are due to the subtractive measurement technique for ΣANs. Both gas- and aerosol-phase organic nitrate concentrations continue to increase after the limonene is completely consumed. Little nitric acid (≤2 ppb) was observed over this 24-h experiment. After the consumption of limonene, NO_3 and N_2O_5 are observed to gradually build up in the chamber, as NO_2 and O_3 continue to be present in high concentration.

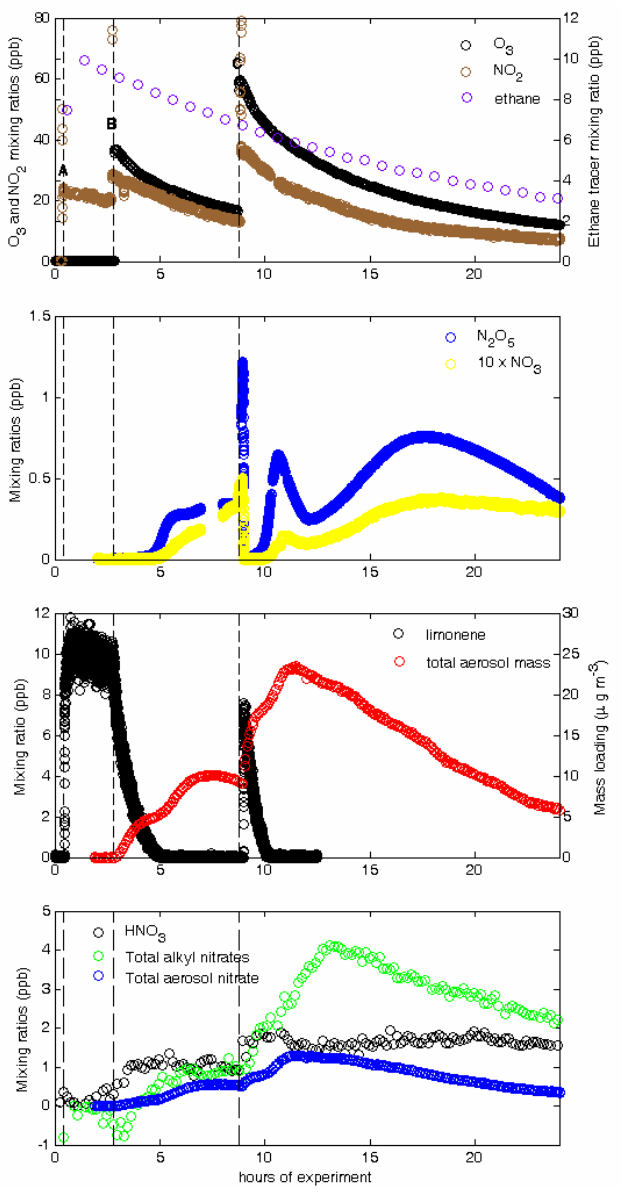

Fig. 1. Overview time series of species monitored. Ethane was used as an inert dilution tracer. Chamber temperature was between 288–296 K for the duration of this experiment. Dashed vertical lines refer to key changes in chamber composition, described in detail in the text. At **(A)**, first limonene was injected; at **(B)**, oxidative chemistry was initiated by addition of ozone; at **(C)**, a second batch of limonene and oxidants was injected.

Four hours following the complete consumption of limonene, the SAPHIR chamber, now containing $\approx$10 µg m^{-3} of "seed" organic aerosol, was re-charged, bringing the NO_2 concentration to 38 ppb and O_3 to 60 ppb, followed by addition of $\approx$10 ppb of limonene (label (c) in Fig. 1). (Note: although 10 ppb limonene was injected, a peak of only 7 ppb was observed due to slow mixing relative to rapid oxidation. Thermal dissociation of N_2O_5 gives an instantaneous source of NO_3, such that during these first minutes, oxidation is largely NO_3 driven.) We observed immediate and sustained production of organic nitrates and aerosol, with significantly higher ultimate yields of both, compared to those after the first injection. NO_3 and N_2O_5 concentrations were again observed to build up in the chamber after the limonene had been completely consumed. Then, approximately one hour into this buildup, NO_3 and N_2O_5 decrease again for several hours, corresponding to a period where the highest organic nitrate concentrations and highest aerosol mass were observed.

4 Analysis

4.1 Organic nitrate yield

The organic nitrate yields (= branching ratio of organic nitrate channel) after oxidation of the two double bonds in limonene are different. Following each injection of limonene, two time-separated sequential increases in organic nitrate concentration were observed: the first while the limonene concentration was decreasing, and the second after all limonene precursor had reacted away. Organic nitrate formation requires NO_3 reaction, as there is not any NO in the chamber to react with RO_2. During the second increase NO_3 may be oxidizing products of either the limonene + O_3 or the limonene + NO_3 reaction. In the first oxidation step, 50% of the limonene reacted with O_3, the remainder with NO_3.

We assume that the endocyclic bond reacts with NO_3 about thirty times faster than the exocyclic double bond, based on proxy alkenes (see Sect. 5). To our knowledge, separate rate constants for NO_3 with the two double bonds in limonene have not been measured.

The absolute organic nitrate yield of the NO_3 + limonene reaction can be estimated from instantaneous changes in $\Sigma RONO_2$ signal coincident with titration of limonene. The apparent nitrate yield during limonene consumption ($\Delta\Sigma RONO_2/\Delta$Limonene) is approximately 15% for both limonene injections, but this ignores the reaction of 50% of the limonene with O_3. Hence, the initial alkyl nitrate yield from NO_3 + limonene reactions alone is approximately 30%.

The alkyl nitrate yield (including additional nitrate production after the complete consumption of limonene) is variable between the two injections. The net alkyl nitrate formed after the first and second injections of 10 ppb limonene were 1 and 3 ppb, corresponding to overall nitrate yields of 10% and 30%, respectively; however, as discussed below, the later formation of gaseous organic nitrate is complicated.

4.2 Aerosol mass yield

Aerosol formation was observed after each of two limonene injections. To determine aerosol yield, we first correct the

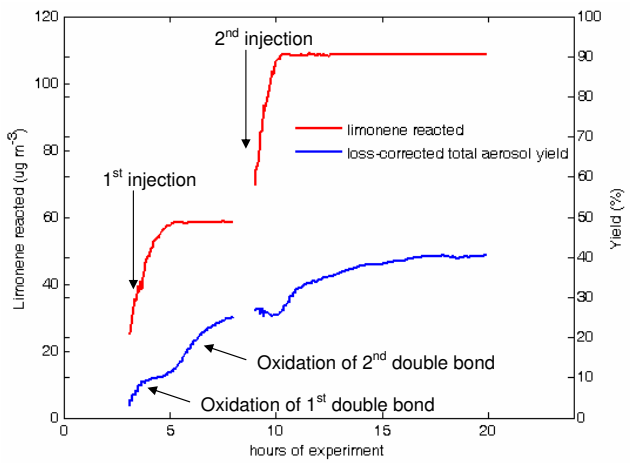

Fig. 2. Total limonene reacted and time-dependent, loss-corrected total aerosol yield for the two limonene injections. Increase in yield after limonene is depleted indicates that reaction at the second double bond in first-generation oxidation products produces aerosol.

aerosol mass loading for dilution and wall losses. We then calculate the mass yield as:

$$Y = \frac{\Delta M}{\Delta \mathrm{VOC}} \quad (1)$$

where ΔM is the corrected aerosol mass loading ($\mu g\,m^{-3}$) and ΔVOC is the total reacted concentration ($\mu g\,m^{-3}$) of limonene. The yields are determined relative to each of the two separate injections of limonene, i.e., SOA formed from the first injection is simply considered "background" aerosol for the second injection. The final SOA yields observed (Fig. 2) at the peak aerosol concentration following each injection were 25% for the first injection and 40% after the second injection, suggesting that the presence in the second case of $10\,\mu g\,m^{-3}$ of existing aerosol from the first injection enhanced partitioning to the aerosol phase.

As seen in Eq. (1), these *mass-based* yields are calculated relative to limonene reacted. Hence, it is important in the interpretation of these yields to recall that oxidation of both double bonds in limonene adds significant additional mass to the molecule. If we assume the average molecular weight of aerosol-forming species is $250\,g\,mole^{-1}$, corresponding to limonene ($C_{10}H_{16}$) with addition of a nitrate group (NO_3) and hydroxyl group (OH), the yield on a per-molecule basis would be 14–22%.

Following the first limonene injection, the relative SOA yields from two generations of oxidation (the oxidation of first the endo-, then the exocyclic double bonds in limonene) can be observed (Fig. 2), separated by their differing timescale. Oxidation of the first double bond in limonene by O_3 and NO_3 results in a 10% yield of SOA. The necessity for very low volatility nucleating species in this initial aerosol formation contributed to the low mass yield; while after the second injection, products of intermediate volatility could condense onto pre-existing aerosol.

Both limonene injections show relatively low initial gas-phase nitrate yields, measured as the increase in TD-LIF observed $\Sigma RONO_2$ divided by the decrease in limonene. This indicates that NO_3-limonene reactions preferentially form the non-nitrate ketone product channels. Nevertheless, these reactions constitute an efficient pathway for SOA formation. On average, 15% of the aerosol mass is constituted of nitrate (NO_3, mW = 62).

5 Interpretation

5.1 Proposed reaction mechanism

Limonene is oxidized by both NO_3 and O_3, as outlined in the mechanism shown in Fig. 3. The two double bonds in limonene allow the possibility of at least two NO_3 oxidation steps, each of which can produce an organic nitrate or non-nitrate; for simplicity we assume that the non-nitrate channel produces a ketone. This assumption is based on ketones being the highest yield non-nitrate product observed in reactions of NO_3 with a variety of alkenes (Table III-D-1, Calvert et al., 2000). Either double bond can also react with O_3, the products of which have been determined in other chamber studies (Maksymiuk et al., 2009): the major O3LIM product is a C_{10} backbone with a carbonyl and a carboxyl functional group added. As the limonene backbone becomes increasingly oxidized, these products can partition to the aerosol phase, generating SOA. We construct a mechanism and use observations to constrain the poorly known parameters, including the relative rates of NO_3 oxidation of the first and second double bond, the branching ratio of organic nitrate vs. ketone formation, and the gas-aerosol partitioning of the oxidation products.

5.1.1 Gas-phase kinetics

The full reaction scheme shown above (Fig. 3) is explicitly modeled with rate constants as tabulated in Table 2. Each double bond reacts with either NO_3 or O_3, at both first and second generations of oxidation.

In a base case model, we assume the non-specific rate constant measured for NO_3 + limonene was the rate for the faster reaction at the endocyclic double bond ($1.2 \times 10^{-11}\,cm^3\,molec^{-1}\,s^{-1}$ at 298 K, Calvert et al. (2000), chamber temperature ranged 294–296 K during the oxidation, so no temperature dependence was assumed). We apply the ratio of the measured rate constants for NO_3 with 2-methyl-propene ($3.1 \times 10^{-13}\,cm^3\,molec^{-1}\,s^{-1}$, proxy for the exocyclic double bond) to NO_3 with 2-methyl-2-butene ($9.3 \times 10^{-12}\,cm^3\,molec^{-1}\,s^{-1}$, proxy for the endocyclic double bond) to determine the rate of the slower reaction at the exocyclic double bond ($4.0 \times 10^{-13}\,cm^3\,molec^{-1}\,s^{-1}$). The measured

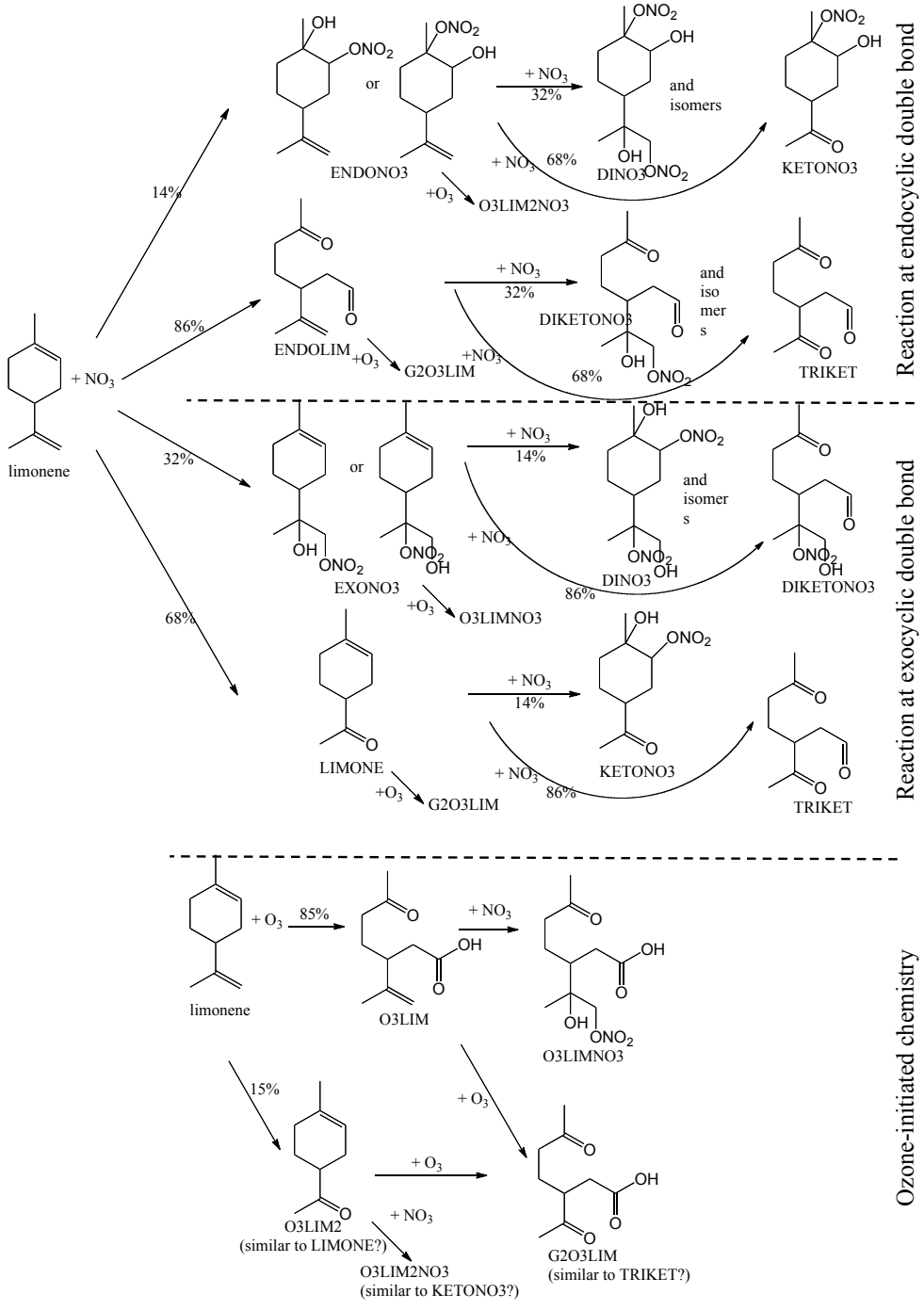

Fig. 3. Reaction scheme of NO_3 and O_3 oxidation of limonene. Structures (especially O_3 products) are proposed approximations; names correspond to individual molecular species tracked in model mechanism.

O_3 + limonene rate of 2.0×10^{-16} cm^3 molec^{-1} s^{-1} (Calvert et al., 2000) is assumed to be the total rate constant for both double bonds, with the reaction occurring 15% of the time at exocyclic double bond and 85% of the time at the endocyclic double bond, following Leungsakul et al. (2005). Applying instead the factor of 30 between rate constants at the two double bonds derived by another recent study (Donahue et al., 2007) does not significantly affect results; essentially only the major product channel influences subsequent chemistry in either case. Reactions of O_3 or NO_3 with first-generation oxidation products of limonene are assumed to proceed at the same rate as on limonene

itself, i.e., oxidation of one double bond does not affect rate constants at the other double bond. This is in contrast to recent studies on isoprene nitrates (Lockwood et al., 2010), which found that the nitrate group β to the double bond increased its reaction rate with O_3. Since in this case the double bonds are separated by three bonds, we assume the effect is negligible.

The reaction of NO_3 with aldehydes produced in early generations of the chemistry are also important. The rate constants used here are estimated based on a comprehensive study of the kinetics of NO_3 reaction with a series of aldehydes (D'Anna et al., 2001).

Wall loss rates of reactive species are determined from the timescale of NO_3, O_3, and N_2O_5 loss in an earlier VOC-free chamber experiment, and aerosol loss rates from observed particle number density decay during this experiment. Values for the branching ratios for nitrate versus ketone production at each NO_3 oxidation step are assumed to be independent of other functional groups on the molecule. The organic nitrate branching ratios are estimated to be 32% at the exo double bond and 14% at the endo double bond, based on overall nitrate branching ratios for α- and β-pinene in the Master Chemical Mechanism v3.1 (Saunders et al., 2003).

In this base case model, NO_3 and N_2O_5 are always underpredicted, while organic nitrate is initially over predicted (after the first limonene addition, hours 4–7) and later underpredicted (hours 9–24). The model/measurement discrepancy is improved by systematically adjusting a number of the parameters in the gas phase mechanism, subject to observational constraints, which are summarized in Table 1.

Since the concentrations of NO_3 and N_2O_5 are determined by their source (R1) and sinks, and the source is well constrained, we adjust the modeled NO_3 sinks to find the best agreement between modeled and measured NO_3 and N_2O_5 after limonene has fully reacted after the first injection (hours 4–7, Fig. 4). The primary sinks of NO_3 are reaction with limonene and its oxidation products. We find the best agreement using rate constants for NO_3 with limonene and its oxidation products that are a factor of two lower than the recommended value of 1.22×10^{-11} cm^3 molec^{-1} s^{-1} $\pm$ 35% (Calvert et al., 2000). The literature measurements of this rate constant span the range 9.4×10^{-12} to 1.31×10^{-11} (Atkinson et al., 1984; Barnes et al., 1990; Martinez et al., 1999); however, our fit value of 6.0×10^{-12} is lower than all previous measurements.

During the first limonene oxidation event, consumption of limonene by O_3 was appreciable relative to NO_3 oxidation (approximately 50% of the limonene is consumed by ozone), since the O_3 was injected after limonene and therefore the NO_3 + limonene reaction was limited by the NO_3 production rate. We observe organic nitrate products to appear immediately in both gas and aerosol phase.

Finally, we tune the unknown rate constant of the larger aldehydes formed in the oxidation mechanism, TRIKET, G2O3 and DIKETONO3, with NO_3using the total HNO_3 produced in the experiment ($\approx$ 2 ppb) as a constraint, since these are the sole sources of nitric acid. We find the rate of NO_3 + TRIKET or DIKETONO3 to be 50 times the rate of NO_3 + HCHO, a reasonable range for a larger aldehyde (D'Anna et al., 2001).

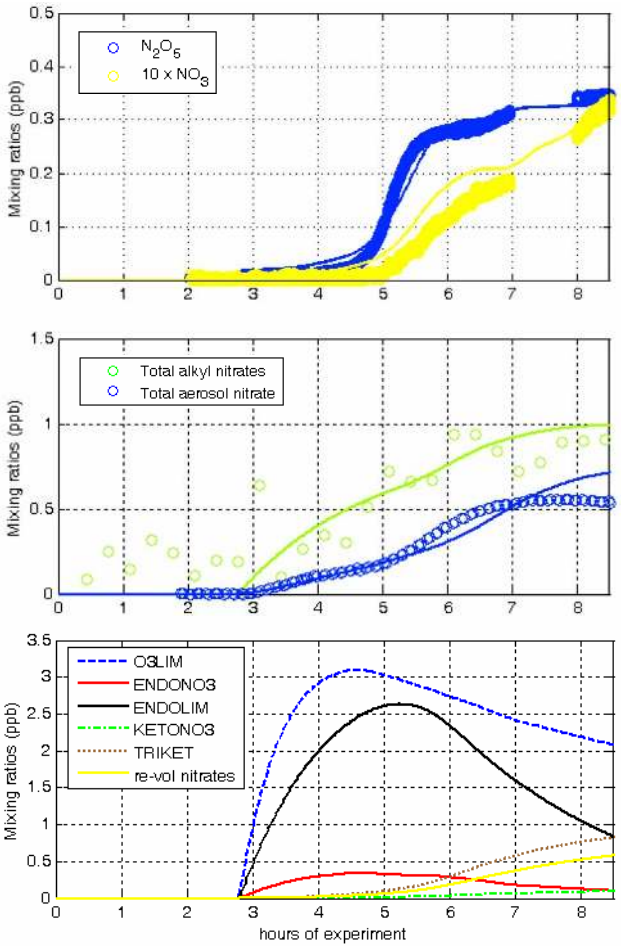

Fig. 4. Measured (markers) and modeled (lines) time traces after the first limonene injection. Bottom panel shows the major products modeled.

These three constraints result in gas-phase chemistry that reproduces the concentrations after the first limonene injection reasonably well (Fig. 4). However, we note that the model overestimates NO_3 and that the second pulse of aerosol nitrate is overpredicted by about 30% before the second limonene injection (at hour 9).

5.1.2 Modeling aerosol partitioning of condensing species

We model the gas-aerosol partitioning of the limonene oxidation products using the equilibrium absorptive partitioning formalism, following Pankow and Capouet (Pankow, 1994;

Table 1. Parameters that were tuned in this model to best fit the observational data, along with the observational constraints used to determine best fit.

Tuned parameter	Observational constraint	Value used in model
Rate of NO_3 + LIM	Limonene decay; total NO_3 + N_2O_5, hours 4–7	6.0×10^{-12} cm^3 molec^{-1} s^{-1}
Rate of NO_3 + O3LIM	Alkyl nitrate formation after 1st injection	0
Ratio of rates of NO_3 + endo vs. exo C = C	Overall NO_3/N_2O_5 shape after 1st injection	30
Rate of NO_3 + later-gen. aldehydes	HNO_3 production	50 × NO_3 + HCHO rate
Tuning factors for all p_{vap}	Gas/aerosol partitioning of nitrate after 1st injection; organic/nitrate aerosol loading	See Table 3
$\gamma_{NO_3-aerosol}$	Gas/aerosol partitioning of nitrate after 2nd injection	0.2

Table 2. Reaction rate constants and branching ratios used in gas-phase portion of kinetics box model. For structures corresponding to variable names, see reaction scheme figure.

Reaction	Branching ratio	Rate constant (cm^{3}molecule^{-1}s^{-1}, 298 K unless otherwise indicated)	Reference/Notes
$NO_2 + O_3 \rightarrow NO_3$		JPL T-dependent rate; 3.2×10^{-17}	JPL Kinetics Eval 15, July 2007
$NO_3 + NO_2 \rightarrow N_2O_5$		JPL T-dependent rate; 1.0×10^{-12}	JPL Kinetics Eval 15, July 2007
$N_2O_5 \rightarrow NO_3 + NO_2$		$2.13\times10^{-27}\times\exp(11025/T)$	Based on equilibrium constant measured at Juelich, July 2007
NO_3 + LIM → ENDONO3	0.14	6.0×10^{-12}	Calvert et al., 2000 (÷ 2)
NO_3 + LIM → ENDOLIM + NO2	0.86	6.0×10^{-12}	ibid.
NO_3 + LIM → EXONO3	0.32	2.0×10^{-13}	Above ÷ 30, see text
NO_3 + LIM → LIMONE + HCHO	0.68	2.0×10^{-13}	ibid.
NO_3 + EXONO3 → DINO3	0.14	6.0×10^{-12}	Same as rate at endo bond in bare limonene
NO_3 + EXONO3 → DIKETONO3	0.86	6.0×10^{-12}	ibid.
NO_3 + LIMONE → KETONO3	0.14	6.0×10^{-12}	ibid.
NO_3 + LIMONE → TRIKET	0.86	6.0×10^{-12}	ibid.
NO_3 + ENDONO3 → DINO3	0.32	2.0×10^{-13}	Same as rate at exo bond in bare limonene
NO_3 + ENDONO3 → KETONO3 + HCHO + NO2	0.68	2.0×10^{-13}	ibid.
NO_3 + ENDOLIM → DIKETONO3	0.32	2.0×10^{-13}	ibid.
NO_3 + ENDOLIM → TRIKET	0.68	2.0×10^{-13}	ibid.
NO_3 + TRIKET → G3KET + HNO3		2.9×10^{-14}	50 × rate of NO_3 + HCHO; see text
NO_3 + G2O3 → G3O3 + HNO3		2.9×10^{-14}	ibid.
NO_3 + DIKETONO3 → G3NO3 + HNO3		2.9×10^{-14}	ibid.
O_3 + LIM → O3LIM (endo)		1.7×10^{-16}	85% of total O_3 + LIM, Calvert et al., 2000
O_3 + LIM → O3LIM2 (exo)		3.0×10^{-17}	15% of total O_3 + LIM, Calvert et al., 2000
O_3 + O3LIM → G2O3 = TRIKET		3.0×10^{-17}	Same as rate at exo bond in bare limonene
O_3 + O3LIM2 → G2O3 = TRIKET		1.7×10^{-16}	Same as rate at endo bond in bare limonene
NO_3 + O3LIM → O3LIMNO3		$< 4.0\times10^{-15}$	Rate of NO_3 + LIM (exo) ÷ 50 is upper limit; see text
NO_3 + O3LIM2 → O3LIM2NO3 = KETONO3		$< 1.2\times10^{-13}$	Rate of NO_3 + LIM (endo) ÷50 is upper limit; see text
O_3 + ENDONO3 → O3LIM2NO3 = KETONO3		3.0×10^{-17}	Same as rate at exo bond in bare limonene
O_3 + ENDOLIM → G2O3 = TRIKET		3.0×10^{-17}	Same as rate at exo bond in bare limonene
O_3 + EXONO3 → O3LIMNO3 = DIKETONO3		1.7×10^{-16}	Same as rate at endo bond in bare limonene
O_3 + LIMONE → G2O3 = TRIKET		1.7×10^{-16}	Same as rate at endo bond in bare limonene
NO_3 + walls →		6.0×10^{-4}	from NO_3 loss timescale in VOC-free chamber
N_2O_5 + walls →		7.2×10^{-5}	from N_2O_5 loss timescale in VOC-free chamber
O_3 + walls →		3.9×10^{-6}	from O_3 loss timescale in VOC-free chamber
limonene oxidation products + walls →		1.8×10^{-5}	fit to later alkyl nitrate decay

Capouet and Müller, 2006):

$$K_p = \frac{F/\mathrm{TSP}}{A} = \frac{760 \cdot R \cdot T \cdot f_{\mathrm{om}}}{\mathrm{MW_{om}} \cdot 10^6 \cdot \zeta \cdot p_{\mathrm{vap}}} \quad (2)$$

F and A are the total aerosol-phase and gaseous concentrations of the compound of interest, and TSP is the concentration of total suspended particulate matter. In the second expression showing the equilibrium constant in terms of thermodynamic properties, R is the universal gas constant ($8.314\,\mathrm{J\,mol^{-1}\,K^{-1}} = 8.206\times10^{-5}\,\mathrm{atm\,m^3\,K^{-1}\,mol^{-1}}$), T is temperature (K), f_{om} is the weight fraction of organic matter in the total aerosol (=1 for these experiments), $\mathrm{MW_{om}}$ is

the average molecular weight of the absorbing organic material (g mol^{-1}), ζ is the activity coefficient of the compound of interest in the condensed phase (assumed = 1 for these experiments), and p_{vap} is the subcooled vapor pressure of the compound of interest (Torr); 760 (Torr atm^{-1}) and 10^6 (µg g^{-1}) are conversion factors. This gives K_p in units of m^3 µg^{-1}.

We explicitly model the equilibrium gas/aerosol partitioning of 11 condensable species: EXONO3/ENDONO3 (same p_{vap}), DINO3, KETONO3/O3LIM2NO3 (same p_{vap}), DIKETONO3/O3LIMNO3 (same p_{vap}), TRIKET, G2O3, and O3LIM/O3LIM2 (same p_{vap} assumed for O_3 product from either double bond). For each, we calculate p_{vap} based on the proposed product structures shown in Fig. 3 and the group contribution method of Pankow and Asher (2008). These calculated values and the tuned values used in the present model are reported in Table 3. To initiate aerosol formation, a small amount of "seed" aerosol is injected in the model at the moment of ozone injection into the limonene; the seed does not affect ultimate aerosol yield in this equilibrium model. Partitioning is implemented by determining the gas-phase and aerosol fractions of each species at each time step, assuming that this partitioning is effectively instantaneous.

As has been noted in previous studies (Leungsakul et al., 2005; Fry et al., 2009), the predicted vapor pressures underestimates the aerosol produced. This suggests that the actual structures of limonene oxidation products are either more oxidized or oligomerized forms of the proposed structures, or that the group contribution method overestimates vapor pressure. Because the bulk oxidation state of the modeled species agrees with AMS observations (see Sect. 5.3), it seems unlikely that additional oxidation is the explanation for these underestimates.

We employ the observed mass loading of organic and nitrate aerosol from the AMS as well as the observed gas/aerosol partitioning of organic nitrate after the first limonene injection as constraints to determine tuning factors to apply to the values of p_{vap} used in the model. The shape of the time trace allows distinction between first- and second-generation oxidation products. Measurement/model agreement on the organic and nitrate aerosol loading before and after tuning vapor pressures are shown in Fig. 5. After determining the tuning factors that best approximate the experimental data, the same group contribution method can be used to rationalize those factors applied. Most striking is the need for both first- and second-generation NO_3 products to have significantly lower volatility.

Initially, only one-fifth the observed aerosol nitrate after the first limonene injection was produced in the model. The vapor pressures were fit to the first nine hours of observed gas and aerosol phase nitrates, greatly improving measurement/model agreement (Fig. 4). This is a function both of the reduced vapor pressures of the nitrates themselves, and of having in general more organic aerosol mass onto which organic nitrates can partition.

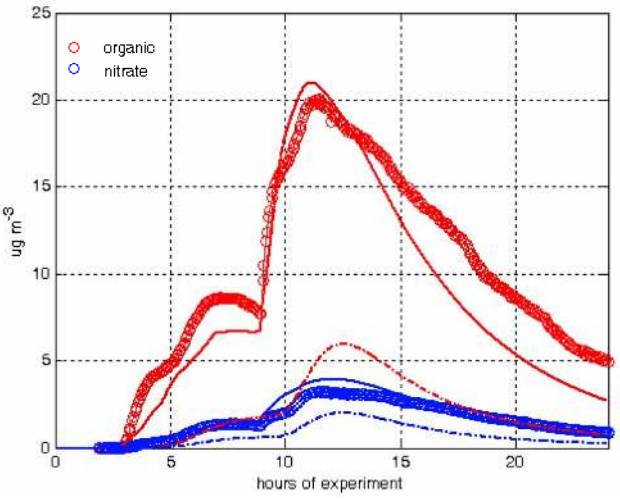

Fig. 5. Change in measurement/model agreement of AMS-measured aerosol organic and aerosol nitrate mass loading before (dashed lines) and after (solid) tuning predicted vapor pressures.

5.2 Interpreting nitrate and aerosol formation after second limonene injection

Kinetic modeling captures limonene consumption by NO_3 and O_3, initial alkyl nitrate yields, overall aerosol yield and organic to nitrate ratio of the aerosol produced. However, the agreement between model and experimental observations of NO_3 shown in Fig. 4 does not persist through the second limonene injection. Without further changes, the gas-phase organic nitrate from hour 10 onwards is drastically underpredicted, while NO_3 is overpredicted. Because the maximum discrepancy coincides with the highest aerosol loading, reaction of NO_3 on the surface of the organic aerosol to produce an $RONO_2$ species that is more volatile than its parent aerosol-bound VOC is suggested. We model the aerosol uptake of NO_3 using:

$$k_{uptake} = \frac{\gamma \, v_{NO_3} \, SA}{4} \quad (3)$$

where γ is the unitless uptake coefficient, v_{NO_3} is the molecular speed of NO_3 (cm s^{-1}), and SA is the total aerosol surface area per volume (cm^2 cm^{-3}) calculated from the modeled aerosol mass, assumed density (1.6 g cm^{-3}, Fry et al., 2009) and measured mode particle radius (AMS). For the purposes of this modeling, we assume the limiting case: that every organic nitrate produced by this reaction evaporates to the gas phase. We multiply SA by the (modeled) fraction of aerosol containing unsaturated double bonds to more easily enable comparison to uptake measurements on well-defined hydrocarbon surfaces. With the observed and modeled aerosol surface area peaking at 1.3×10^{-6} cm^2 cm^{-3}, an uptake coefficient of NO_3 onto the fraction of the aerosol that contains double bonds of $\gamma \approx 5 \times 10^{-1}$ provides the best fit

Table 3. Parameters used in gas-aerosol partitioning portion of the kinetics box model. Calculated vapor pressures were determined using the formalism of Pankow and Asher (2008). For reference, the p_{vap} determined for a pinene monohydroxynitrate was 4.0×10^{-5} Torr (Fry et al., 2009).

Parameter	Calculated value (Torr)	Adjusted value (Torr)
p_{vap}(EXONO3 and ENDONO3)	2.9×10^{-5}	5.8×10^{-7}
p_{vap}(DINO3)	8.2×10^{-10}	8.2×10^{-11}
p_{vap}(KETONO3)	9.6×10^{-6}	9.6×10^{-7}
p_{vap}(DIKETONO3 and O3LIMNO3)	5.0×10^{-7}	5.0×10^{-9}
p_{vap}(TRIKET)	5.8×10^{-3}	5.8×10^{-3}
p_{vap}(O3LIM)	7.4×10^{-5}	7.4×10^{-6}
p_{vap}(G2O3)	3.1×10^{-5}	3.1×10^{-6}

to the gas/aerosol nitrate partitioning after the 2nd limonene injection (Fig. 6). This uptake coefficient was determined using observed NO_3; the figure shows the resulting improvement of fit in the full model using this γ. In this experiment, the double-bond containing fraction of the aerosol ranges between 10% and 40%, meaning the uptake coefficient on the total aerosol formed in the SAPHIR chamber ranged between $\gamma = 0.05$–0.2.

The availability of these aerosol-phase double bonds for heterogeneous reaction with NO_3 relies on their not being rapidly consumed by O_3. This was found to be the case by Zhang et al. (2006), who observed rapid ozone uptake by limonene SOA under low-NO_x conditions, but *not* under high-NO_x conditions. Hence, in the present experiments, without ozone scavenging, the unsaturated aerosol-phase organics remain available for NO_3 uptake.

The derived value of NO_3 uptake coefficient (γ= 0.05–0.2) is in general agreement with the results of Gross et al. (2009), who measured uptake coefficients around 2×10^{-3} on neat liquid surfaces of saturated ethers and polyols, up to 2×10^{-1} for a mono-unsaturated carboxylic acid. Under the dry conditions of the present experiment, heterogeneous uptake of N_2O_5 was expected to be negligible. In our previous study on SOA formation from $NO_3 + \beta$-pinene (Fry et al., 2009), we found that we did not need to include any heterogeneous chemistry to explain observations. This is reasonable, since in that study the aerosol formed by NO_3 reaction with the monounsaturated alkene would not have contained double bonds. Given the low aerosol surface area in that study and using the measured uptake coefficient for NO_3 on saturated alkanes of around 10^{-3} (Gross et al., 2009; Moise et al., 2002), the heterogeneous loss rate of NO_3 was negligibly small. In contrast, in this limonene experiment the aerosol contains some unsaturated double bonds, as shown in our proposed mechanism. In addition to the chemistry we have outlined, it is possible that efficient $RO_2 + RO_2$ chemistry leads to formation of condensable unsaturated organic peroxides, such as those observed by Ng et al. in the case of NO_3 oxidation of isoprene (Ng et al., 2008). The existence of double bonds in the aerosol phase leads to a higher uptake coefficient in this case and significant heterogeneous NO_3 uptake.

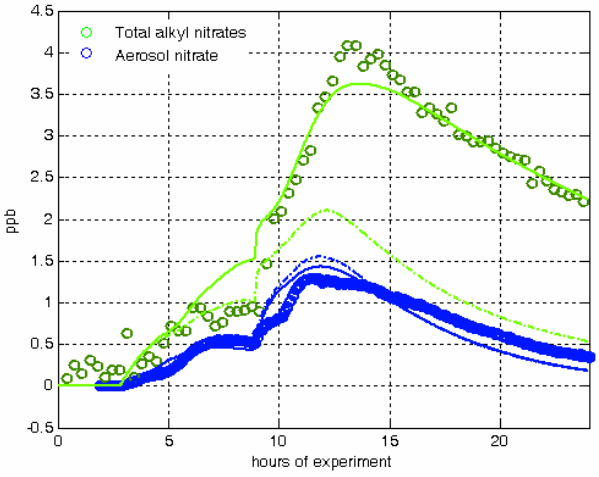

Fig. 6. Change in measurement/model agreement of aerosol and total nitrate without (dashed lines) and with (solid) inclusion in the model of NO_3 uptake and revolatilization of organic nitrate. An uptake coefficient of $\gamma = 0.5$ onto the double-bond containing fraction of aerosol gives the best agreement, equivalent to an overall uptake coefficient on this aerosol of $\gamma = 0.05$–0.2. While the addition of this uptake process does not appreciably change the modeled nitrate aerosol, it does drops peak organic aerosol concentrations by about 5 µg m^{-3}, from 26 to 21 µg m^{-3}. The optimized model traces in Fig. 5 include this uptake process.

Given the underpredicted aerosol formation from our raw reaction mechanism, this model is almost certainly incomplete in terms of later oxidation steps. Therefore, it is possible that a late-peaking gas-phase species is instead responsible for this very efficient observed conversion of NO_3 to volatile organic nitrate; however, as will be shown below, there is additional evidence in the AMS data for consumption

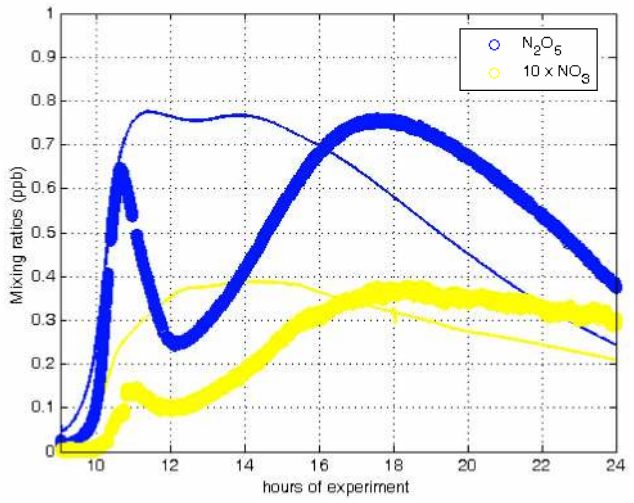

Fig. 7. Measurement/model agreement of NO_3 and N_2O_5 after the second limonene injection. No reasonable permutations of model parameters achieved better agreement with the NO_3 "dip".

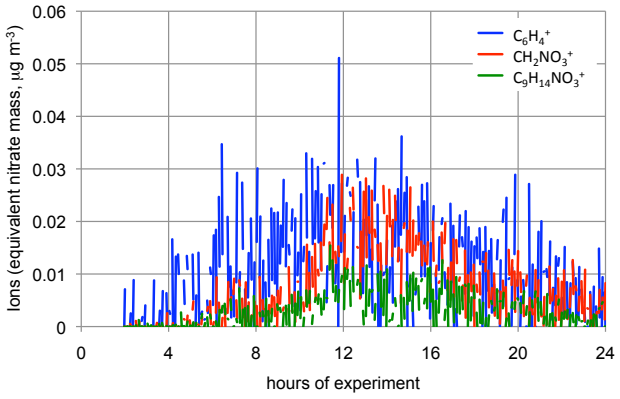

Fig. 8. AMS-detected organo-nitrates fragments. For reference, $C_6H_4^+$ is also shown, a fragment which occurs at the same nominal *m/z* as $CH_2NO_3^+$.

of organic aerosol that bolsters this hypothesis of heterogeneous NO_3 reactions.

Despite the improvement in modeling gas/aerosol partitioning of organic nitrate with this heterogeneous process included, no reasonable permutations on the rate constants or partitioning constants of mechanism described thus far can fully reproduce the major unique feature of this "second experiment": the pronounced dip in NO_3 and N_2O_5 around 12 h. This dip was observed by multiple instruments. Figure 7 shows the measured and modeled NO_3 and N_2O_5 with the complete model described here. A slight dip appears due to the heterogeneous uptake of NO_3, but not nearly as abrupt nor with as dramatic a recovery as observed in the data. We have attempted increasing the rate of that process, as well as all other NO_3 sinks in the present mechanism. In all cases, this further depletes NO_3/N_2O_5 everywhere rather than simply deepening the dip. What appears to be necessary is a chemical process that is activated only at hour 11 and ceases at hour 13. Hour 12 of the experiment corresponds to 18:00 UTC, but continuous measurements of NO show no change during this time period, ruling out the possibility that low-angle sunlight leaked into the chamber. This NO_3 dip remains a major gap in the modeling of this system, which we have not been able to resolve with the mechanism described here.

It is notable that the remaining discrepancy between measured and modeled alkyl nitrate (Fig. 6, green data and solid line) is essentially identical in magnitude, opposite in sign, and synchronous in time with the discrepancy between measured and modeled N_2O_5 (Fig. 7, blue traces). What remains mysterious is what process could induce this *temporary* source of volatile alkyl nitrate intermediate.

Table 1 summarizes all tuned parameters in the gas and aerosol model and the observations used to constrain each.

5.3 Aerosol chemical composition

As in previous investigations of the SOA formation from reactions of NO_3 with biogenic VOCs (β-pinene, Fry et al. (2009) and isoprene, Rollins et al., 2009), the main characteristic feature of the organic nitrates is a low NO^+/NO_2^+ ratio. In addition, the *m/z* 76 ($CH_2NO_3^+$) ion fragment again appears as an indicator for the presence of organic nitrates. Beyond this, the AMS observations diverge from previous experiments somewhat. Here, a heavier *m/z* 184 ($C_9H_{14}NO_3^+$) fragment is clearly present throughout the experiment (Fig. 8). The increase in this fragment over the course of the experiment suggests that larger nitrates are incorporated into the aerosol via later-generation chemistry.

Comparison of bulk atomic composition of the SOA observed by the AMS (Aiken et al., 2008) to calculated composition based on the surrogate model compounds reveals broad agreement on the level of oxidation of the aerosol components. Both measurement and model have an average O/C ratio of about 0.4, increasing gradually over the course of the experiment (observed O/C rises from about 0.3 to 0.45). This suggests that the model chemistry at least accurately captures the bulk oxidation level of the condensing species.

In order to further assess SOA chemistry (ozonolysis versus NO_3 oxidation sources, first versus second generation oxidation), the AMS organic aerosol fraction was analysed using positive matrix factorization (PMF) (Paatero and Tapper, 1994; Paatero, 1997). This analysis was performed entirely independent of the above described kinetics modeling. The PMF analysis applied principles and utilized code as introduced by Ulbrich et al. (2009). The number of factors used to describe the total aerosol formed was selected based on the residuals both in MS and time space. Since the sources for

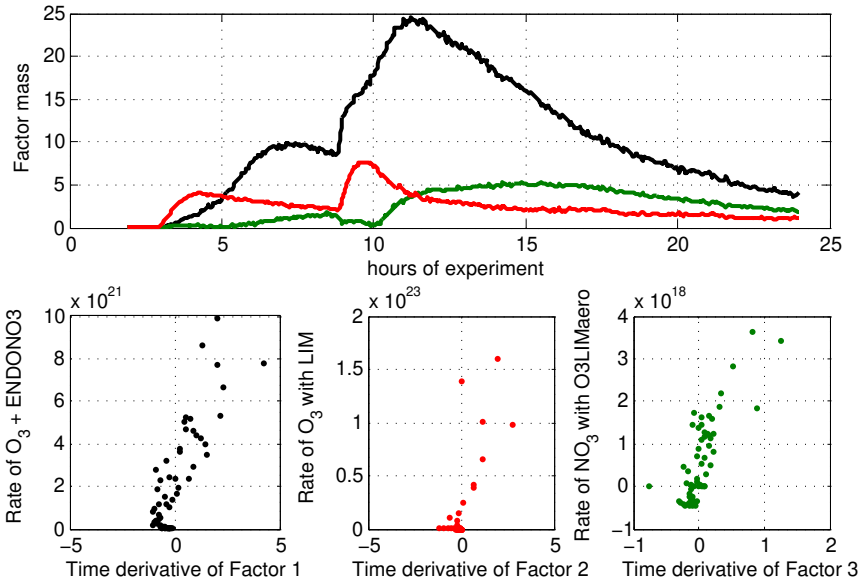

Fig. 9. Summary of PMF results. Upper panel: measured mass in each factor (1: black, 2: red, and 3: green). After these three mass factors, residuals were below +/−2% for the entire experiment. Lower panels: correlation plots of the time derivative of each factor with the rate of the best correlated chemical process.

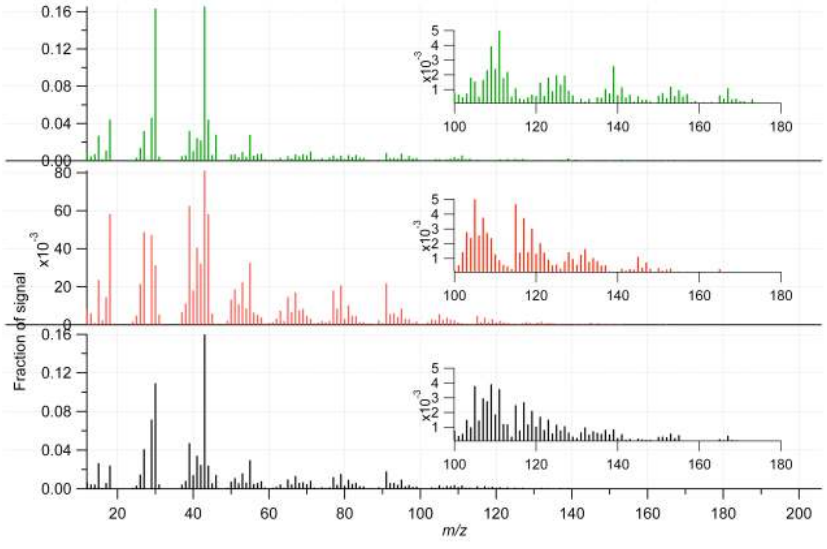

Fig. 10. Mass spectra of the three factors derived from PMF analysis with inserts showing expanded views. Factor one (black) is characterized by a large contribution from *m/z* 43 and significant 30 and 46. Factor two (red) has a significant signal on *m/z* 44 and 39, suggesting oxidized organics, and has no contribution from the nitrate masses. Factor three (green) has the largest relative contribution from nitrate masses and larger contributions on *m/z* >100 than factor 1.

aerosol formation were reactions of limonene with $NO_3$and O_3, the nitrate that was observed in the course of the experiment was included in the PMF analysis. Three factors were found to describe the measured data with residuals below 2% at all times (Fig. 9).

The resolved PMF components (Fig. 10) can be interpreted based upon the correlation of their time derivatives with rates of selected processes based on modeled species. Factor 1 has high nitrate content (*m/z* 30 and 46 contribute 12% to the factor 1 mass), and the ratio of 46/30 is 0.13, well below the typical ratio observed for NH_4NO_3. It is also

correlated to the AMS measured nitrate ($R^2 = 0.95$) and is thus interpreted as organic nitrate. Of the modeled organic nitrate production rates, factor 1 correlates poorly with first-generation production ([NO3] × [LIM], $R^2 = 0.46$), but correlates well with second-generation production from ozone oxidation of first generation nitrates ([O3] × [ENDONO3], $R^2 = 0.83$). It is not at all correlated with NO_3 oxidation of first-generation ozone products.

The second factor is better correlated with first-generation ozone oxidation of limonene ([O3] × [LIM], $R^2 = 0.73$) than second-generation ([O3] × [O3LIM], $R^2 = 0.26$). Its mass spectral pattern supports the interpretation of oxidized organics from the first generation reaction of O_3 with limonene.

The third component also contains significant organic nitrate: the ratio of 46/30 is 0.17 for factor 3 and the sum of 30 and 46 contribute 19% of the total mass of this factor. It is best correlated with reaction of NO_3 with ozone-produced aerosol ([NO3] × [O3LIMaero], $R^2 = 0.73$). A correlation almost as good is found using [NO3] × SA, weighted by factor 2 ($R^2 = 0.61$), which was attributed to the purely ozone-generated aerosol. We therefore interpret factor 3 as representing heterogeneous uptake processes on the SOA in the second part of the experiment. The decay of the organic factor 2 coincident with increase in this factor also supports this interpretation. It is possible that NO_3 uptake onto limonene SOA results sometimes in revolatilization of an organic nitrate (as invoked in this model), sometimes in net uptake of nitrate, creating larger multifunctional nitrates which remain in the aerosol phase, and sometimes in NO_2 release and chemical conversion of the aerosol phase.

6 Conclusions

Observations of the reaction of NO_3 with limonene show that the $RONO_2$ yield is approximately 30%, implying significant release of the nitrate functional group after attack at the double bonds. The aerosol mass yield is 25–40%. We find that aerosol composition is affected by NO_3 reaction with increased incorporation of organic nitrate into the aerosol over time and apparent conversion of aerosol bound alkene moieties to nitrate moieties. These conclusions bolster other recent evidence suggesting that nitrate addition to monoterpenes may be an important player in the aerosol budget in those locations where biogenic terpene emissions are large and NO_x is abundant.

Acknowledgements. The Berkeley authors were supported by NSF ATM-0639847 and NSF ATM-0511829. The authors thank the entire SAPHIR NO_3 intercomparison campaign team, June 2007 at Forschungszentrum Jülich, for their support of these experiments. This work was a joint activity of the European Network of Excellence ACCENT (contract no: GOCE CT-2004-505337) and EUROCHAMP.

Edited by: J. N. Crowley

References

Aiken, A. C., DeCarlo, P. F., Kroll, J. H., Worsnop, D. R., Huffman, J. A., Docherty, K. S., Ulbrich, I. M., Mohr, C., Kimmel, J. R., Sueper, D., Sun, Y., Zhang, Q., Trimborn, A., Northway, M., Ziemann, P. J., Canagaratna, M. R., Onasch, T. B., Alfarra, M. R., Prevot, A. S. H., Dommen, J., Duplissy, J., Metzger, A., Baltensperger, U., and Jimenez, J. L.: O/C and OM/OC Ratios of Primary, Secondary, and Ambient Organic Aerosols with High-Resolution Time-of-Flight Aerosol Mass Spectrometry, Environ. Sci. Technol., 42, 4478–4485, 2008.

Allan, J., Delia, A., Coe, H., Bower, K., Alfarra, M., Jimenez, J., Middlebrook, A., Drewnick, F., Onasch, T., Canagaratna, M., Jayne, J., and Worsnop, D.: A Generalised method for the extraction of chemically resolved mass spectra from aerodyne aerosol mass spectrometer data, J. Aerosol Sci., 35, 909–922, 2004.

Apel, E. C., Brauers, T., Koppmann, R., Bandowe, B., Boßmeyer, J., Holzke, C., Tillmann, R., Wahner, A., Wegener, R., Brunner, A., Jocher, M., Ruuskanen, T., Spirig, C., Steigner, D., Steinbrecher, R., Gomez Alvarez, E., Müller, K., Burrows, J. P., Schade, G., Solomon, S. J., Ladstätter-Weißenmayer, A., Simmonds, P., Young, D., Hopkins, J. R., Lewis, A. C., Legreid, G., Reimann, S., Hansel, A., Wisthaler, A., Blake, R. S., Ellis, A. M., Monks, P. S., and Wyche, K. P.: Intercomparison of oxygenated volatile organic compound measurements at the SAPHIR atmosphere simulation chamber, J. Geophys. Res., 113, D20(307), doi:10.1029/2008JD009865, 2008.

Apodaca, R., Dorn, H.-P., Ball, S. M., Brauers, T., Brown, S. S., Cohen, R. C., Crowley, J., Dorn, H.-P., D. W., Fry, J. L., Fuchs, H., Haseler, R., Heitmann, U., Kato, S., Kajii, Y., Kiendler-Scharr, A., Kleffmann, J., Labazan, I., Matsumoto, J., Nishida, S., Rollins, A. W., Tillmann, R., Wahner, A., Wegener, R., Wooldridge, P. J., and Simpson, W. R.: Intercomparison of N_2O_5 sensors using SAPHIR reaction chamber, Atmos. Chem. Phys., in preparation, 2011.

Atkinson, R., Aschmann, S. M., Winer, A. M., and Pitts, J. N. J.: Kinetics of the Gas-Phase Reactions of NO_3 Radicals with a Series of Dialkenes, Cycloalkenes, and Monoterpenes at 295 ± 1 K, Environ. Sci. Technol., 18, 370–375, 1984.

Barnes, I., Bastian, V., Becker, K. H., and Tong, Z.: Kinetics and Products of the Reactions of NO_3 with Monoalkenes, Dialkenes, and Monoterpenes, J. Phys. Chem., 94, 2413–2419, 1990.

Bateman, A. P., Nizkorodov, S. A., Laskin, J., and Laskin, A.: Time-resolved molecular characterization of limonene/ozone aerosol using high-resolution electrospray ionization mass spectrometry, Phys. Chem. Chem. Phys., 11, 7931–7942, doi:10.1039/b905288g, 2009.

Bohn, B. and Zilken, H.: Model-aided radiometric determination of photolysis frequencies in a sunlit atmosphere simulation chamber, Atmos. Chem. Phys., 5, 191–206, doi:10.5194/acp-5-191-2005, 2005.

Calvert, J., Atkinson, J., Kerr, J., Madronich, S., Moortgat, G. K., Wallington, T., and Yarwood, G.: Mechanisms of the atmospheric oxidation of the alkenes, Oxford University Press, New York, NY, 2000.

Canagartna, M., Jayne, J., Jimenez, J., Allan, J., Alfarra, M., Zhang, Q., Onaxch, T., Drewnick, F., Coe, H., Middlebrook, A., Delia, A., Williams, L., Trimborn, A., Northway, M., DeCarlo, P., Kolb, C., Davidovits, P., and Worsnop, D.: Chemical and microphysical characteriation of ambient aerosols with the aerodyne aerosol

mass spectrometer, Mass Spectrom. Rev., 26, 185–222, 2007.

Capouet, M. and Müller, J.-F.: A group contribution method for estimating the vapour pressures of a-pinene oxidation products, Atmos. Chem. Phys., 6, 1455–1467, doi:10.5194/acp-6-1455-2006, 2006.

D'Anna, B., Andresen, O., Gefen, Z., and Nielsen, C. J.: Kinetic study of OH and NO_3 radical reactions with 14 aliphatic aldehydes, Phys. Chem. Chem. Phys., 3, 3057–3063, 2001.

Day, D. A., Wooldridge, P. J., Dillon, M., Thornton, J. A., and Cohen, R. C.: A thermal dissociation laser-induced fluorescence instrument for in situ detection of NO_2, peroxy nitrates, alkyl nitrates, and HNO_3, J. Geophys. Res., 107, D64046, doi:10.1029/2001JD000779, 2002.

de Gouw, J. A., Middlebrook, A. M., Warneke, C., Goldan, P. D., Kuster, W. C., Roberts, J. M., Fehsenfeld, F. C., Worsnop, D. R., Canagaratna, M. R., Pszenny, A. A. P., Keene, W. C., Marchewka, M., Bertman, S. B., and Bates, T. S.: Budget of organic carbon in a polluted atmosphere: Results from the New England Air Quality Study in 2002, J. Geophys. Res.-Atmos., 110, D16305, doi:10.1029/2004JD005623, 2005.

Donahue, N. M., Tischuk, J. E., Marquis, B. J., and Huff Hartz, K. E.: Secondary organic aerosol from limona ketone: insights into terpene ozonolysis via synthesis of key intermediates, Phys. Chem. Chem. Phys., 9, 2991–2998, doi:10.1039/b701333g, 2007.

Dorn, H. P., Apodaca, R., Ball, S., Brauers, T., Brown, S. S., Cohen, R. C., Crowley, J., Dube, W. P., Fry, J., Fuchs, H., Haseler, R., Heitmann, U., Jones, R., Kato, S., Kajii, Y., Kiendler-Scharr, A., Labazan, I., Matsumoto, J., Meinen, J., Nishida, S., Platt, U., Rohrer, F., Rollins, A., Ruth, A., Schlosser, E., Schuster, G., Shillings, A., Simpson, W., Thieser, J., Tillmann, R., Varma, R., Venables, D., Wahner, A., Wegener, R., and Wooldridge, P. J.: Intercomparison of 10 different NO_3 measurement techniques at the simulation chamber SAPHIR, Atmos. Chem. Phys., in preparation, 2011.

Dube, W. P., Brown, S. S., Osthoff, H. D., Nunley, M. R., Ciciora, S. J., Paris, M. W., McLaughlin, R. J., and Ravishankara, A. R.: Aircraft instrument for simultaneous, in situ measurement of NO_3 and N_2 O_5 via pulsed cavity ring-down spectroscopy, Rev. Sci. Instrum., 77, 034101, doi:10.1063/1.2176058, 2006.

Eerdekens, G., Yassaa, N., Sinha, V., Aalto, P. P., Aufmhoff, H., Arnold, F., Fiedler, V., Kulmala, M., and Williams, J.: VOC measurements within a boreal forest during spring 2005: on the occurrence of elevated monoterpene concentrations during night time intense particle concentration events, Atmos. Chem. Phys., 9, 8331–8350, doi:10.5194/acp-9-8331-2009, 2009.

Fry, J. L., Kiendler-Scharr, A., Rollins, A. W., Wooldridge, P. J., Brown, S. S., Fuchs, H., Dubé, W., Mensah, A., dal Maso, M., Tillmann, R., Dorn, H.-P., Brauers, T., and Cohen, R. C.: Organic nitrate and secondary organic aerosol yield from NO_3 oxidation of β-pinene evaluated using a gas-phase kinetics/aerosol partitioning model, Atmos. Chem. Phys., 9, 1431–1449, doi:10.5194/acp-9-1431-2009, 2009.

Fuchs, H., Dubé, W., Ciciora, S., and Brown, S.: Determination of Inlet Transmission and Conversion Efficiencies for in Situ Measurements of the Nocturnal Nitrogen Oxides, NO_3, N_2O_5 and NO_2 via Pulsed Cavity Ring-Down Spectroscopy, Anal. Chem., 80, 6010–6017, 2008.

Fuchs, H., Ball, S. M., Bohn, B., Brauers, T., Cohen, R. C., Dorn, H.-P., Dubé, W. P., Fry, J. L., Häseler, R., Heitmann, U., Jones, R. L., Kleffmann, J., Mentel, T. F., Msgen, P., Rohrer, F., Rollins, A. W., Ruth, A. A., Kiendler-Scharr, A., Schlosser, E., Shillings, A. J. L., Tillmann, R., Varma, R. M., Venables, D. S., Villena Tapia, G., Wahner, A., Wegener, R., Wooldridge, P. J., and Brown, S. S.: Intercomparison of measurements of NO_2 concentrations in the atmosphere simulation chamber SAPHIR during the NO3Comp campaign, Atmos. Meas. Tech., 3, 21–37, doi:10.5194/amt-3-21-2010, 2010.

Goldstein, A. H. and Galbally, I. E.: Known and Unexplored Organic Constituents in the Earth's Atmosphere, Environ. Sci. Tech., 41(5), 1514-1521, 2007.

Griffin, R. J., Cocker, D. R., Flagan, R. C., and Seinfeld, J. H.: Organic aerosol formation from the oxidation of biogenic hydrocarbons, J. Geophys. Res.-Atmos., 104, 3555–3567, 1999.

Gross, S., Iannone, F., Xiao, S., and Bertram, A.: Reactive uptake studies of NO_3 and N_2O_5 on alkenoic acid, alkanoate, and polyalcohol substrates to probe nighttime aerosol chemistry, Phys. Chem. Chem. Phys., 11, 7792–7803, 2009.

Guenther, A., Hewitt, C. N., Erickson, D., Fall, R., Geron, C., Graedel, T., Harley, P., Klinger, L., Lerdau, M., McKay, W. A., Pierce, T., Scholes, B., Steinbrecher, R., Tallamraju, R., Taylor, J., and Zimmerman, P.: A global model of natural volatile organic compound emissions, J. Geophys. Res., 100, 8873–8892, doi:10.1029/94JD02950, 1995.

Hallquist, M., Wangberg, I., Ljungstrom, E., Barnes, I., and Becker, K. H.: Aerosol and product yields from NO_3 radical-initiated oxidation of selected monoterpenes, Environ. Sci. Technol., 33, 553–559, 1999.

Hoyle, C. R., Boy, M., Donahue, N. M., Fry, J. L., Glasius, M., Guenther, A., Hallar, A. G., Huff Hartz, K., Petters, M. D., Petäjä, T., Rosenoern, T., and Sullivan, A. P.: A review of the anthropogenic influence on biogenic secondary organic aerosol, Atmos. Chem. Phys., 11, 321–343, doi:10.5194/acp-11-321-2011, 2011.

Lane, T. E., Donahue, N. M., and Pandis, S. N.: Simulating secondary organic aerosol formation using the volatility basis-set approach in a chemical transport model, Atmos. Env., 42, 7439–7451, doi:10.1016/j.atmosenv.2008.06.026, 2008.

Leungsakul, S., Jaoui, M., and Kamens, R.: Kinetic mechanism for predicting secondary organic aerosol formation from the reaction of d-limonene with ozone, Env. Sci. Technol., 39, 9583–9594, doi:10.1021/es0492687, 2005.

Lindinger, W., Hansel, A., and Jordan, A.: Proton-transfer-reaction mass spectrometry (PTR-MS): on-line monitoring of volatile organic compounds at pptv levels, Chem. Soc. Rev., 27, 347–354, 1998.

Lockwood, A. L., Shepson, P. B., Fiddler, M. N., and Alaghmand, M.: Isoprene nitrates: preparation, separation, identification, yields, and atmospheric chemistry, Atm. Chem. Phys., 10, 6169–6178, doi:10.5194/acp-10-6169-2010, 2010.

Maksymiuk, C. S., Gayahtri, C., Gil, R. R., and Donahue, N. M.: Secondary organic aerosol formation from multiphase oxidation of limonene by ozone: mechanistic constraints via two-dimensional heteronuclear NMR spectroscopy, Phys. Chem. Chem. Phys., 11, 7810–7818, doi:10.1039/b820005j, 2009.

Martinez, E., Cabanas, B., Aranda, A., Martin, P., and Salgado, S.: Absolute rate coefficients for the gas-phase reactions of NO_3 radical with a series of monoterpenes at $T = 298$ to 433 K, J. Atmos. Chem., 33, 265–282, 1999.

Moise, T., Talukdar, R. K., Frost, G. J., Fox, R. W., and Rudich, Y.: Reactive uptake of NO_3 by liquid and frozen organics, J. Geophys. Res., 107, D24014 doi:10.1029/2001JD000334, 2002.

Ng, N. L., Kwan, A. J., Surratt, J. D., Chan, A. W. H., Chhabra, P. S., Sorooshian, A., Pye, H. O. T., Crounse, J. D., Wennberg, P. O., Flagan, R. C., and Seinfeld, J. H.: Secondary organic aerosol (SOA) formation from reaction of isoprene with nitrate radicals (NO_3), Atmos. Chem. Phys., 8, 4117–4140, doi:10.5194/acp-8-4117-2008, 2008.

Paatero, P.: Least squares formulation of robust non-negative factor analysis, Chemometrics and Intelligent Laboratory Systems, 37, 23–35, 3rd International Conference on Environmetrics and Chemometrics, LAS VEGAS, NV, SEP 11–13, 1995, 1997.

Paatero, P. and Tapper, U.: Positive matrix factorization - a nonnegative factor model with optimal utilization of error-estimates of data values, Environmetrics, 5, 111–126, 1994.

Pankow, J. F.: An Absorption-Model of Gas-Particle Partitioning of Organic-Compounds in the Atmosphere, Atmos. Environ., 28, 185–188, 1994.

Pankow, J. F. and Asher, W. E.: SIMPOL.1: a simple group contribution method for predicting vapor pressures and enthalpies of vaporization of multifunctional organic compounds, Atmos. Chem. Phys., 8, 2773–2796, doi:10.5194/acp-8-2773-2008, 2008.

Pye, H. O. T., Chan, A. W. H., Barkley, M. P., and Seinfeld, J. H.: Global modeling of organic aerosol: the importance of reactive nitrogen, Atmos. Chem. Phys. Discuss., 10, 21259–21301, doi:10.5194/acpd-10-21259-2010, 2010.

Quinn, P. K., Bates, T. S., Coffman, D., Onasch, T. B., Worsnop, D., Baynard, T., de Gouw, J. A., Goldan, P. D., Kuster, W. C., Williams, E., Roberts, J. M., Lerner, B., Stohl, A., Pettersson, A., and Lovejoy, E. R.: Impacts of sources and aging on submicrometer aerosol properties in the marine boundary layer across the Gulf of Maine, J. Geophys. Res., 111, D23S36, doi:10.1029/2006JD007582, 2006.

Ridley, B., Grahek, F., and Walega, J.: A small, high-senstivitiy, medium-response ozone detector suitable for measurements from light aircraft, J. Atmos. Ocean Tech., 9, 142–148, 1992.

Rohrer, F., Bohn, B., Brauers, T., Brning, D., Johnen, F.-J., Wahner, A., and Kleffmann, J.: Characterisation of the photolytic HONO-source in the atmosphere simulation chamber SAPHIR, Atmos. Chem. Phys., 5, 2189–2201, doi:10.5194/acp-5-2189-2005, 2005.

Rollins, A. W., Kiendler-Scharr, A., Fry, J., Brauers, T., Brown, S. S., Dorn, H.-P., Dubé, W. P., Fuchs, H., Mensah, A., Mentel, T. F., Rohrer, F., Tillmann, R., Wegener, R., Wooldridge, P. J., and Cohen, R. C.: Isoprene oxidation by nitrate radical: alkyl nitrate and secondary organic aerosol yields, Atmos. Chem. Phys. Discuss., 9, 8857–8902, doi:10.5194/acpd-9-8857-2009, 2009.

Sakulyanontvittaya, T., Duhl, T., Wiedinmyer, C., Helmig, D., Matsunaga, S., Potosnak, M., Milford, J., and Guenther, A.: Monoterpene and sesquiterpene emission estimates for the United States, Env. Sci. Technol., 42, 1623–1629, doi:10.1021/es702274e, 2008.

Saunders, S. M., Jenkin, M. E., Derwent, R. G., and Pilling, M. J.: Protocol for the development of the Master Chemical Mechanism, MCM v3 (Part A): tropospheric degradation of non-aromatic volatile organic compounds, Atmos. Chem. Phys., 3, 161–180, doi:10.5194/acp-3-161-2003, 2003.

Schichtel, B., Malm, W., Bench, G., Fallon, S., McDade, C., Chow, J., and Watson, J.: Fossil and contemporary fine particulate carbon fractions at 12 rural and urban sites in the United States, J. Geophys. Res., 113, D02311, doi:10.1029/2007JD008605, 2008.

Schlosser, E., Brauers, T., Dorn, H.-P., Fuchs, H., Häseler, R., Hofzumahaus, A., Holland, F., Wahner, A., Kanaya, Y., Kajii, Y., Miyamoto, K., Nishida, S., Watanabe, K., Yoshino, A., Kubistin, D., Martinez, M., Rudolf, M., Harder, H., Berresheim, H., Elste, T., Plass-Dülmer, C., Stange, G., and Schurath, U.: Technical Note: Formal blind intercomparison of OH measurements: results from the international campaign HO × Comp, Atmos. Chem. Phys., 9, 7923–7948, 2009, http://www.atmos-chem-phys.net/9/7923/2009/.

Slowik, J. G., Stroud, C., Bottenheim, J. W., Brickell, P. C., Chang, R. Y.-W., Liggio, J., Makar, P. A., Martin, R. V., Moran, M. D., Shantz, N. C., Sjostedt, S. J., van Donkelaar, A., Vlasenko, A., Wiebe, H. A., Xia, A. G., Zhang, J., Leaitch, W. R., and Abbatt, J. P. D.: Characterization of a large biogenic secondary organic aerosol event from eastern Canadian forests, Atmos. Chem. Phys., 10, 2825–2845, doi:10.5194/acp-10-2825-2010, 2010.

Spittler, M., Barnes, I., Bejan, I., Brockmann, K. J., Benter, T., and Wirtz, K.: Reactions of NO3 radicals with limonene and alpha-pinene: Product and SOA formation, Atmos. Environ., 40, S116–S127, doi:10.1016/j.atmosenv.2005.09.093, 2006.

Thornton, J. A., Wooldridge, P. J., and Cohen, R. C.: Atmospheric NO_2: In situ laser-induced fluorescence detection at parts per trillion mixing ratios, Anal. Chem., 72, 528–539, 2000.

Tunved, P., Hansson, H., Kerminen, V., Strom, J., Dal Maso, M., Lihavainen, H., Viisanen, Y., Aalto, P., Komppula, M., and Kulmala, M.: High natural aerosol loading over boreal forests, Science, 312, 261–263, doi:10.1126/science.1123052, 2006.

Ulbrich, I. M., Canagaratna, M. R., Zhang, Q., Worsnop, D. R., and Jimenez, J. L.: Interpretation of organic components from Positive Matrix Factorization of aerosol mass spectrometric data, Atmos. Chem. Phys., 9, 2891–2918, doi:10.5194/acp-9-2891-2009, 2009.

Wainman, T., Zhang, J., Weschler, C., and Lioy, P.: Ozone and limonene in indoor air: A source of submicron particle exposure, Environ. Health Pers., 108, 1139–1145, 2000.

Weber, R. J., Sullivan, A. P., Peltier, R. E., Russell, A., Yan, B., Zheng, M., de Gouw, J., Warneke, C., Brock, C., Holloway, J. S., Atlas, E. L., and Edgerton, E.: A study of secondary organic aerosol formation in the anthropogenic-influenced southeastern United States, J. Geophys. Res.-Atmos., 112, D13302, doi:10.1029/2007JD008408, 2007.

Wegener, R., Brauers, T., Koppmann, R., Bares, S. R., Roher, F., Tillmann, R., Wahner, A., Hansel, A., and Wisthaler, A.: Simulation chamber investigation of the reactions of ozone with short-chained alkenes, J. Geophys. Res., 112, D13301, doi:10.1029/2006JD007531, 2007.

Wooldridge, P. J., Perring, A. E., Bertram, T. H., Flocke, F. M., Roberts, J. M., Singh, H. B., Huey, L. G., Thornton, J. A., Wolfe, G. M., Murphy, J. G., Fry, J. L., Rollins, A. W., LaFranchi, B. W., and Cohen, R. C.: Total Peroxy Nitrates (SPNs) in the atmo-

sphere: the Thermal Dissociation-Laser Induced Fluorescence (TD-LIF) technique and comparisons to speciated PAN measurements, Atmos. Meas. Tech., 3, 593–607, doi:10.5194/amt-3-593-2010, 2010.

Zhang, J. Y., Hartz, K. E. H., Pandis, S. N., and Donahue, N. M.: Secondary organic aerosol formation from limonene ozonolysis: Homogeneous and heterogeneous influences as a function of NO_x, J. Phys. Chem. A, 110, 11053–11063, 2006.